Dynamics of growth and detachment of an isolated bubble on an inclined surface

Michel, Thomas Lebon, Julien Sebilleau, Catherine Colin

Dynamics of growth and detachment of an isolated bubble on an inclined surface

M. Lebon,* J. Sebilleau, and C. Colin
Institut de Mécanique des Fluides de Toulouse, Université de Toulouse, CNRS, INPT, UPS, Allée Camille Soula, 31400 Toulouse, France

(Received 20 December 2017; published 3 July 2018)

The quasistatic growth of an air bubble nucleated on an inclined plate is investigated. Three substrates (Teflon, treated glass, and glass) are used to study the influence of the wetting conditions of the plate. The plate has been drilled to allow air injection and nucleation of the bubbles on the substrate. High-speed shadowgraphy visualizations in two perpendicular planes are used to record the evolution of the bubble shape during its growth. Experiments are conducted in quiescent water for different slopes of the plate. The bubble shape is extracted from image processing and several geometric parameters are determined. These geometric parameters are used to evaluate the forces acting on the bubble using a point-force approach. It appears that the classical expressions of the forces are valid for small slopes of the surface (less than 15°), while the force balance is no longer verified for higher slopes. This result is linked to an elongation of the bubble foot that has to be taken into account in the modeling of the capillary force. Thus an expression for the capillary force is proposed and the force balance is used to predict the bubble detachment diameter.

DOI: 10.1103/PhysRevFluids.3.073602

I. INTRODUCTION

Bubble growth on a wall is encountered in many practical situations such as bubble injection through pierced membranes or porous media in gas or liquid contactors in chemical processing, vapor nucleation in evaporators, or inkjet printing devices. In these industrial situations, it is important to predict the bubble size at detachment, which initially controls the interfacial area concentration and thus the transfer of mass, momentum, and energy between the phases. Predicting bubble detachment diameter in boiling is an important issue since most of the mechanistic models for the prediction of heat transfer in nucleated boiling are based on the bubble detachment diameter and frequency [1,2].

In a quiescent liquid, many authors studied experimentally, theoretically, or numerically the gas bubble injection through a capillary tube [3–6] or the vapor bubble on a heated surface [7–11]. In these studies, two main approaches are used to predict the bubble detachment diameter. The first one is based on the integration of the Young-Laplace equation for the calculation of axisymmetric bubble shapes. However, the boundary condition at the bubble foot is different for bubble growth with a pinned contact line and for contact lines that can freely move [12].

The second approach is based on a balance of the forces acting on the bubble: the point-force approach. A classical example of this approach was used by Tate [13] to predict the radius at detachment with a balance between buoyancy and capillary forces. In general, the forces are usually written for spherical bubbles in an infinite medium or in the wall vicinity [14,15]. One advantage of the point-force approach is its ability to predict bubble radius at detachment in situations where the bubble is no longer axisymmetric.

*Corresponding author: michel.lebon01@gmail.com

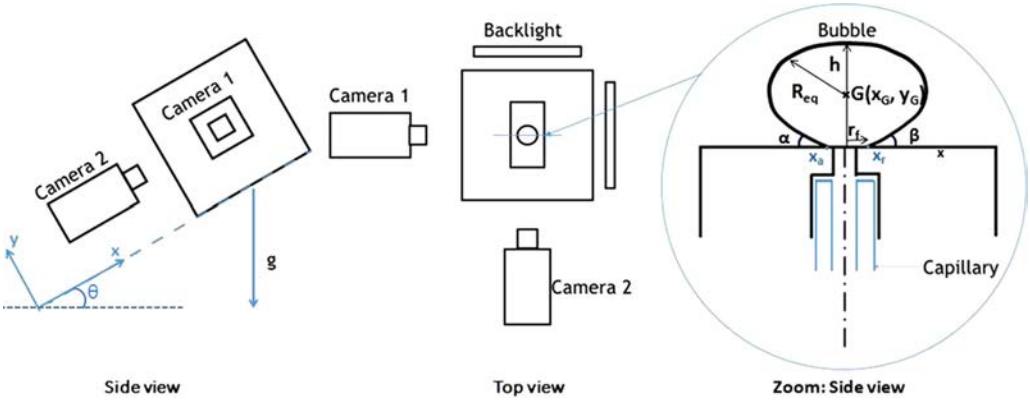

FIG. 1. Experimental setup.

However, in such situations, a modeling of the different forces remains a difficult task. The drag and lift forces exerted by the flow on a bubble growing at the wall are unknown. Another difficulty concerns the modeling of the capillary force, when the bubble is deformed by the flow and its foot elongated. The objective of this study is to improve the modeling of the capillary force on a deformed bubble, when its foot is elongated, in a simple configuration of a bubble growing on an inclined plate in a still liquid. Air bubbles are injected on different substrates and plate inclinations. The capillary force is assessed from a force balance and a modeling is proposed. Finally, a criterion for bubble detachment based on the critical values of the contact angles is proposed.

II. EXPERIMENTAL SETUP AND MEASUREMENT TECHNIQUES

A. Experimental setup

Experiments on bubble injection are performed in a tank (100 mm wide, 100 mm long, and 150 mm high) filled with deionized water at room temperature (20 °C). Air bubbles are injected through a plate by means of a capillary tube of 0.2 mm inner diameter and 1 m in length. The capillary tube edge is 1 mm below the upper plate surface. Thus, the bubble is generated on the substrate. Since the pressure loss inside the capillary tube and through the valves is much higher than the capillary pressure generated by the bubble formation, air is injected with a constant volume flow rate Q throughout the bubble growth. Thus, the equivalent bubble radius evolves as

$$R_{\mathrm{eq}}(t) = \left(\frac{3Qt}{4\pi}\right)^{1/3}. \tag{1}$$

The surface where the bubble is generated can be tilted from $\theta = 0^\circ$ to $\theta = 60^\circ$ (Fig. 1).

Glass windows are incorporated in the four vertical walls of the tank for optical observation. Two high-speed cameras are used in two perpendicular planes to visualize the bubble growth and departure (see Fig. 1).

B. Substrates properties

Experimental conditions (horizontal or tilted substrates) and wetting conditions affect the size, the shape, and contact angles of the bubble but also the sliding or lift-off criterion. At the beginning of the growth, the bubble emerges from the injection hole. Two possibilities can appear: Either the bubble foot remains attached on the edge of the injection hole (good wettability) described by Chesters [12] as the mode A of growth or the foot expands outside of the injection hole (poor wettability) as mode B [12].

TABLE I. Static contact angles.

Substrate	α_{st} (deg)	β_{st} (deg)	$H_d = \alpha_{st} - \beta_{st}$	Roughness (nm)
Teflon	135–140	85–90	50	167
treated glass	108–113	75–84	30	27
normal glass	40–48	10–18	30	6

Experiments are performed on hydrophobic surfaces [Teflon ($r_c = 0.1$ mm, r_c being the cavity radius) or treated glass ($r_c = 0.09$ mm)] or a hydrophilic surface [glass ($r_c = 0.09$ mm)]. As the surface condition (roughness, cleanliness, homogeneity, etc.) can affect the results, we must avoid as much as possible surface irregularities and achieve sufficient cleanliness. For this purpose, the substrate is cleaned with acetone and rinsed with water. Measurements of roughness are carried out using an atomic force microscope. The mean roughness is measured for the three substrates (Table I). The contact angles (Table I) are measured with a tensiometer DSA 100 using drop shape analysis software [16] [the static advancing (receding) contact angle α_{st} (β_{st}) by inflating (aspirating) the drop until the contact line moves forward (backward)]. The glass is hydrophilic ($\alpha_{st_G} = 40^\circ$–48° and $\beta_{st_G} = 10^\circ$–18°). The supersonic particle deposition treatment has been realized by the LAAS on glass substrate leading to hydrophobic conditions ($\alpha_{st_{TG}} = 108^\circ$–$113^\circ$ and $\beta_{st_{TG}} = 75^\circ$–$84^\circ$). The hysteresis angle $H_d = \alpha_{st} - \beta_{st}$ is larger on the Teflon plate due to a higher roughness.

C. Visualization and image processing

The dynamics of the bubble growth and detachment is recorded with two perpendicular high-speed video cameras PCO 1200 HS with 1230×501 pixels at frequencies between 300 and 1000 images per second for different configurations: horizontal surface or inclined surface in a quiescent liquid. All acquisitions are performed by shadowgraphy. The optical axis of camera 1 is set perpendicular to the xy plane (see Fig. 1) and perpendicular to the zy plane for camera 2. The projection of the bubbles on the plane is observed with a spatial resolution of 260 pixels/mm (camera 1) and 295 pixels/mm (camera 2). After experiments, the interface shape of the bubble is digitized with dedicated image processing software, based on MATLAB. The contour of the bubble is determined with different steps of image processing: subtracting the background image, inverting, binarizing, filtering, filling the holes in the bubbles, and extracting the contour of the bubble. Once the profile of the bubble is extracted, the geometrical parameters (see Fig. 1) can be evaluated: equivalent radius R_{eq} based on the bubble volume, foot radius r_f, contact angles α and β, coordinates of the center of gravity in the horizontal and vertical directions x_G and y_G, bubble volume V_b, bubble height h, etc. A polyfit approaches the bubble contour and its derivative at the bubble foot gives the advancing and receding contact angles of the bubble α and β. The contact angles are in good agreement with those obtained with IMAGEJ software and the plug-in drop analysis DropSnake [16]. The bubble volume and its equivalent radius [$(R_{eq} = 3V_b/4\pi)^{1/3}$] are determined considering that the bubble is composed of a stack of circular disks (horizontal surface) or ellipses (tilted surface), 1 pixel high. The minor and major axes of the ellipse are determined with the views of the two cameras on each image. These geometrical parameters are then used to compute the different forces acting on the bubble. We compare the bubble behavior on the different substrates and observe the influence of the wetting conditions on the different geometrical parameters (bubble foot radius, contact angles, bubble equivalent radius, position of the center of gravity, etc.). The calculations were performed on five to ten consecutive bubbles to ensure the reproducibility of the experiments. Only data on an isolated bubble are presented just below.

Measurement errors

At the different steps of image processing, the spatial calibration of the cameras induces an uncertainty of measurement estimated at 0.02 mm on the bubble radius (5% on the bubble volume)

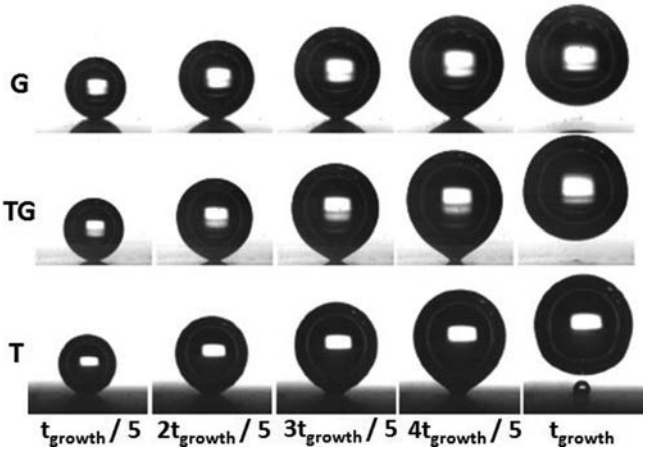

FIG. 2. Growth of a bubble on the three substrates (from top to bottom on camera 1): glass, G; treated glass, TG; and Teflon, T). The view on the second camera is the same for a horizontal surface. Here t_{growth} is the growth time of the bubble until its detachment.

and $\pm 4^\circ$ on the contact angles. The control parameters of the experiment are the inclination angle of the test bench (0°–60°) and the air injection flow rate (0–30 mm^3/s). All experiments are performed for low air injection flow rate, much smaller than the critical flow rate defined by Oguz and Prosperetti [3] and evaluated to 300 mm^3/s. In these conditions, the volume of the bubble at detachment does not depend on the air injection flow rate.

III. EXPERIMENTAL RESULTS

A. Horizontal surface in a quiescent liquid

During its growth, the bubble volume increases and the bubble tends to lift off (Fig. 2). The bubble equivalent radius evolves as $t^{1/3}$ [Fig. 3(b)] following Eq. (1), characteristic of an injection

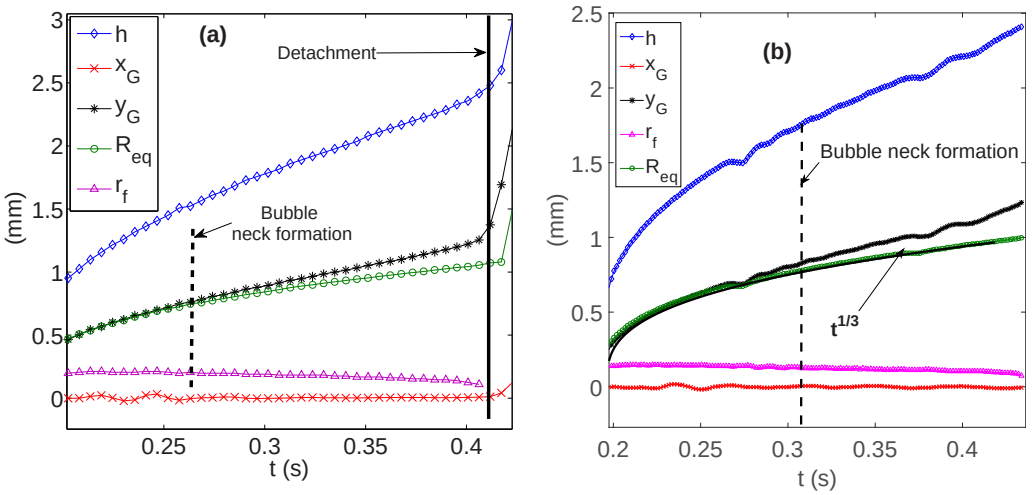

FIG. 3. Horizontal configuration in a quiescent liquid. The evolution of the parameters is shown on (a) the Teflon substrate and (b) the treated substrate.

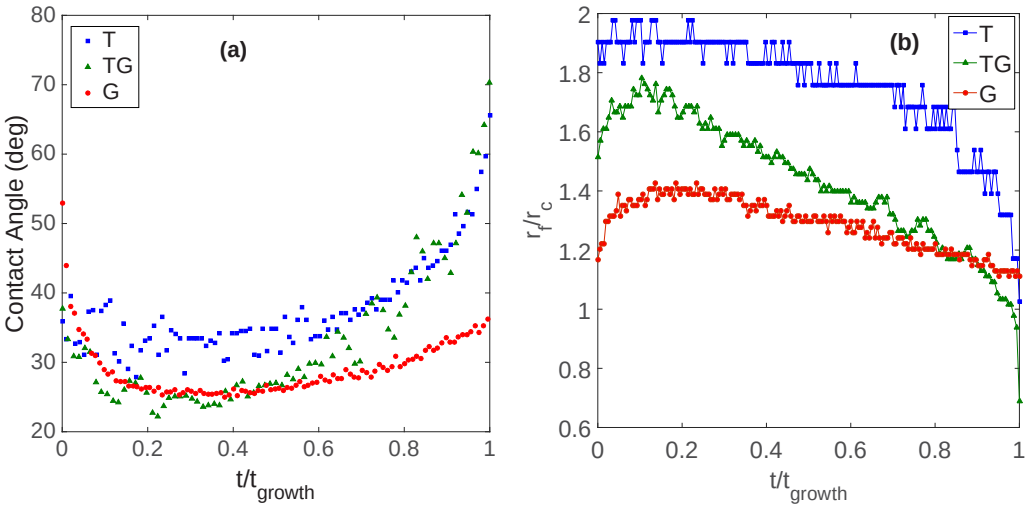

FIG. 4. Evolution of (a) the contact angle and (b) the bubble foot.

at constant volumetric flow rate Q. The flow rate changes between the different experiments but the growth of the bubble is independent of the flow rate (quasistatic regime). The time is scaled by the bubble growth time for comparison. At the beginning of the growth, the bubble has a spherical shape (Fig. 2): The vertical component of the center of gravity y_G follows the equivalent bubble radius R_{eq} (Fig. 3). When it becomes higher than R_{eq}, the bubble loses its spherical shape and a neck appears. An acceleration of the bubble occurs when the bubble begins to detach (see Fig. 3). Indeed, just before detachment, the bubble foot radius decreases [see Figs. 2 and 3(a)].

The influence of the wetting conditions is made apparent by plotting the contact angle evolution and the bubble foot radius for the three substrates (glass, treated glass, and Teflon) in Fig. 4. The bubble foot radius r_f and the time are scaled by the cavity radius r_c and the growth time of the bubble [see Fig. 4(b)].

The Teflon and the treated glass are hydrophobic surfaces. Thus, the bubble expands outside the cavity. The bubble foot radius r_f is higher than the cavity radius r_c ($r_{f_{\text{T}}} > 1.8r_c$ and $r_{f_{\text{TG}}} > 1.5r_c$). For the glass, the ratio between the bubble foot radius and the cavity radius can reach 1.4. Since the plate is hydrophilic, the bubble spreading on the glass plate is less important (Fig. 4). For a perfect and ideal hydrophilic surface, the ratio would be equal to 1 and the contact line would remain pinned on the hole injection edge. The effect of surface wettability can also be seen in Fig. 4(a), where the time evolution of the contact angle is plotted for the three substrates. For hydrophobic surfaces (Teflon and treated glass), the contact angle is larger than for the hydrophilic surface (glass), especially just before bubble detachment. The effect of the surface roughness is also visible in Fig. 4(b), where a stick-slip motion of the contact line can be seen on the Teflon plate. This phenomenon is linked to surface imperfections, the bubble sticks on the wall, and the anchoring and sliding of the triple line occur on defects. The line and the interface are deformed. Beyond a certain deformation, the line detaches from the defect.

For the glass substrates [glass (roughness equal to 6 nm) and treated glass (roughness equal to 27 nm)], the contact line moves constantly. The irregularities present on the surface do not create stick-slip phenomena.

B. Bubble growth on a tilted surface

Several experiments are also performed for different inclination angles between 0° and 60°. The bubble is no longer axisymmetric (Fig. 5). The more the surface inclines, the higher the bubble

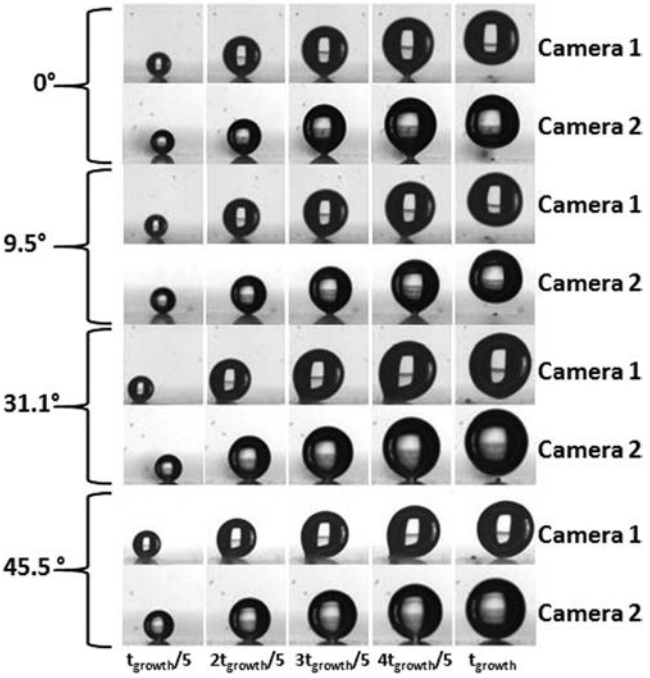

FIG. 5. Experiments on a treated glass plate.

deforms. We show the evolution of the contact angles and the bubble foot radius (on both cameras) versus the inclination angle of the test bench just before the bubble detachment [see Fig. 6(a)]. The difference between advancing and receding contact angles largely increases with the test bench inclination.

Whatever the substrate used, the same changes in these two parameters are observed. On camera 2 (c2), the bubble foot radius is almost constant and is independent of the surface slope [see Fig. 6(b)].

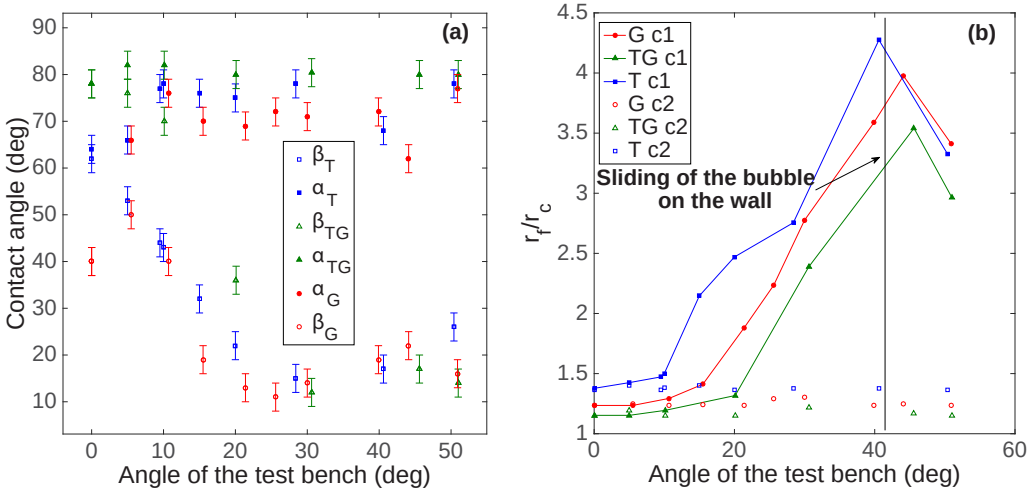

FIG. 6. Evolution of (a) the contact angle at detachment and (b) the bubble foot radius for the three substrates in a tilted surface on c1 (camera 1) and c2 (camera 2).

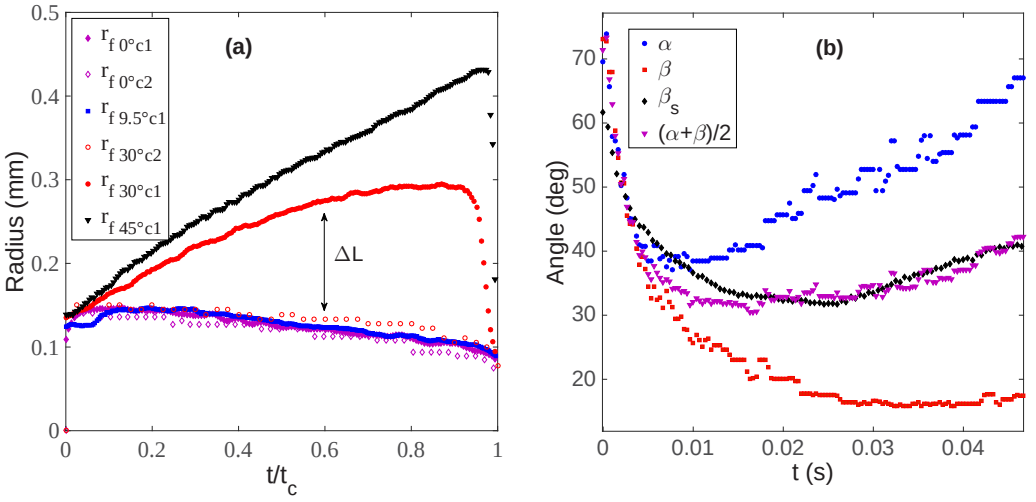

FIG. 7. (a) Evolution of the foot radius r_f for different inclinations of the surface and (b) evolution of the contact angles for a surface tilted of 30°.

For small tilts of the surface (less than 15°), the advancing and receding angles increases and decreases, respectively. The inclination of the surface is too small to see an elongation of the bubble foot radius on camera 1 (c1). The bubble spreads beyond the cavity. When the tilt angle is large enough ($\theta > 15°$), the bubble foot starts expanding. The bubble spreads more and more (see Fig. 6), reaching $r_f = 4.3r_c$ for the Teflon, $r_f = 3.5r_c$ for the treated glass, and $r_f = 4r_c$ for the glass. A decrease of the bubble foot radius is observed for all the substrates tilted at $\theta = 50°$. This is due to the beginning of the bubble sliding. Indeed, beyond a critical angle of the surface, the bubble begins to slide, the triple line retracts, and the radius at the foot bubble decreases. The advancing angle reaches a constant value very quickly (76° for Teflon, 80° for treated glass, and 70° for normal glass) for an angle of inclination of the test bench greater than 10°. The receding contact angle reaches a plateau around 15°–20° for surface inclination superior to 30°.

On a tilted surface, the contact angle evolves all along the contact line, which has to be taken into account in the modeling of the capillary force. On camera 1, the contact angles are different and are called α and β. On camera 2, the contact angles on both sides of the bubble are the same and are called β_s. We plot the evolution of the contact angles on both views [Fig. 7(b)]. The advancing and receding angles respectively increase and decrease, except just before detachment. The evolution of β_s from camera 2 seems to be equal to $\frac{\alpha+\beta}{2}$. Validation of these results for all surface inclinations will be important for the modeling of the capillary force.

The evolution of the bubble foot radius for different surface inclinations is shown in Fig. 7(a) in both views. For clarity, we plot only two inclinations for the second camera. On camera 1 [closed symbols in Fig. 7(a)], at small surface inclination ($\theta < 15°$), the bubble foot radius is almost identical in both views and quickly reaches its maximal value. The bubble foot has a circular shape. For higher inclination of the surface, the bubble foot radius increases more and more until reaching its maximum value at detachment. The bubble has an elongated bubble foot but only in the gravity direction. The elongation of the bubble is called $\Delta L = r_{f_{c1}} - r_{f_{c2}}$. On camera 2 [open symbols in Fig. 7(a)], the bubble foot keeps the same evolution for all inclinations. No elongation is noticed in this direction.

IV. ANALYSIS

We performed the first set of experiments in the most simple situation, a horizontal surface in a quiescent liquid, and then we varied the inclination of the surface. At the beginning of the growth,

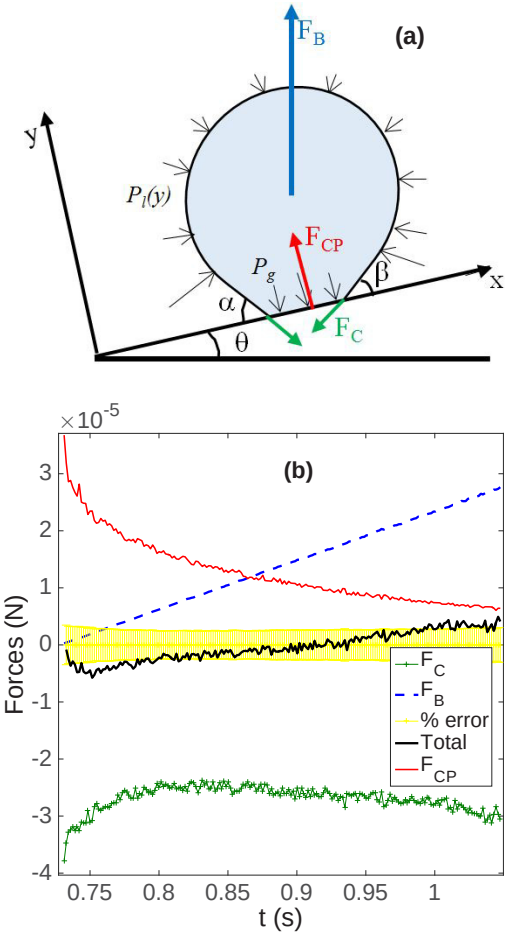

FIG. 8. (a) Forces acting on a bubble. (b) Horizontal surface configuration of forces acting on a bubble on a glass. The error bar in yellow is 10% of the capillary forces.

the bubble has a hemispherical shape, which evolves into a truncated spherical shape and then to an almost spherical shape prior to the formation of a neck at its detachment (Fig. 8). When the surface is tilted, the bubble can be deformed and may slide along the wall before lifting off.

For a bubble growing on its nucleation site in a quiescent liquid (see Fig. 8), the force balance can be written

$$\rho_g V_b \mathbf{g} + \int_{S_b} -P_l \mathbf{n}\, dS + \int_{S_f} -P_g \mathbf{n}\, dS + \mathbf{F_C} = \mathbf{0}, \tag{2}$$

where V_b is the bubble volume, $\mathbf{n}$ is the vector normal to the surface, S_b is the bubble surface S_f the bubble foot surface ($S_f = \pi r_f^2$), $\mathbf{F_C}$ is the capillary force acting at the contact line, and P_l and P_g are the pressure in the liquid and in the gas bubble, respectively. Since the bubble growth is quasistatic, the pressure distribution in the liquid is hydrostatic. Thus drag and inertia forces are neglected. Equation (2) becomes

$$(\rho_g - \rho_l) V_b \mathbf{g} + \int_{S_f} (P_l - P_g) \cdot \mathbf{n}\, dS + \mathbf{F_C} = \mathbf{0}. \tag{3}$$

TABLE II. Calculated volumes in units of mm^3.

Substrate	V_{Tate} [Eq. (7)]	$V_{\text{Tate}\sin(\alpha)}$ [$V_{\text{Tate}}\sin(\alpha)$]	V_{expt}	α_{det} (deg)
Teflon	4.65	4.25	4.51	67
treated glass	4.15	4.02	3.76	77
glass	4.15	2.66	2.58	40

The first term of Eq. (3) is the buoyancy force F_B. It is composed of the weight of the bubble and the Archimedes force.

The second term is the contact pressure force due to the overpressure inside the bubble and to the fact that the bubble is in contact with the wall, instead of being completely surrounded by liquid (see Ref. [14]). This contact pressure force is a function of the pressure difference inside and outside the bubble. The pressure difference across the bubble interface at its foot can be expressed versus the equivalent radius at the bubble top R_S (Laplace equation) and the hydrostatic pressure difference between the bubble top ($y = h$) and the bubble foot ($y = 0$) (see Ref. [17])

$$\mathbf{F_{CP}} = \int_{S_f} (P_l - P_g) \cdot \mathbf{n}\, dS = [P_g(y=0) - P_l(y=0)] S_f \mathbf{e_y}$$
$$= [P_g(y=h) - P_l(y=h) + \rho_l g h] S_f \mathbf{e_y} = \left(\frac{2\gamma_l}{R_S} + \rho_l g h\right) S_f \mathbf{e_y}, \tag{4}$$

where γ_l is the surface tension and S_f the contact surface between the bubble and the wall.

The last term is the capillary force which keeps the bubble foot in contact with the wall. It acts at the triple line (of the solid, liquid, and gas) and is expressed as a function of the polar angle ϕ of the bubble surface in contact with the wall:

$$\mathbf{F_C} = \int_0^{\pi} -2 r_f \gamma_l d\phi\, \boldsymbol{\tau}(\phi), \tag{5}$$

where $\boldsymbol{\tau}$ is the unit vector tangent to the interface and normal to the triple contact line. The buoyancy and the contact pressure promote the bubble detachment, whereas the capillary force keeps the bubble attached to the wall.

A. Horizontal surface

In this case the bubble grows axisymmetrically and the contact angle is constant and equal to α over the circumference of the bubble foot. The surface tension force is thus

$$\mathbf{F_C} = -2\pi r_f \gamma_l \sin(\alpha) \mathbf{e_y}. \tag{6}$$

In the horizontal configuration, the force balance is only in the vertical direction (since $F_{Cx} = F_{Bx} = 0$). We assume that the force balance is satisfied if the sum of the forces is inferior to 10% of the capillary force (see error bars in Fig. 8). The force balance [using Eqs. (4) and (6)] is plotted in Fig. 8 for the glass plate. It is satisfied for this configuration for the three substrates. At the instant of detachment, the contact pressure is small and the buoyancy force balances the capillary force.

In a quasistatic regime, the detachment volume in a quiescent liquid is close to Tate's volume [13]

$$V_{\text{Tate}} = \frac{2\pi \gamma_l r_c}{g(\rho_l - \rho_g)}. \tag{7}$$

For a spherical bubble on a Teflon, treated glass, or glass wall, the volume calculated from the detachment equivalent radius is 4.51, 3.76, and 2.58 mm^3, respectively (Table II). It has an error of 3%, 10%, and 40% by comparison to the volume of Tate ($V_{\text{Tate}} = 4.65$, 4.15, and 4.15 mm^3). Tate's

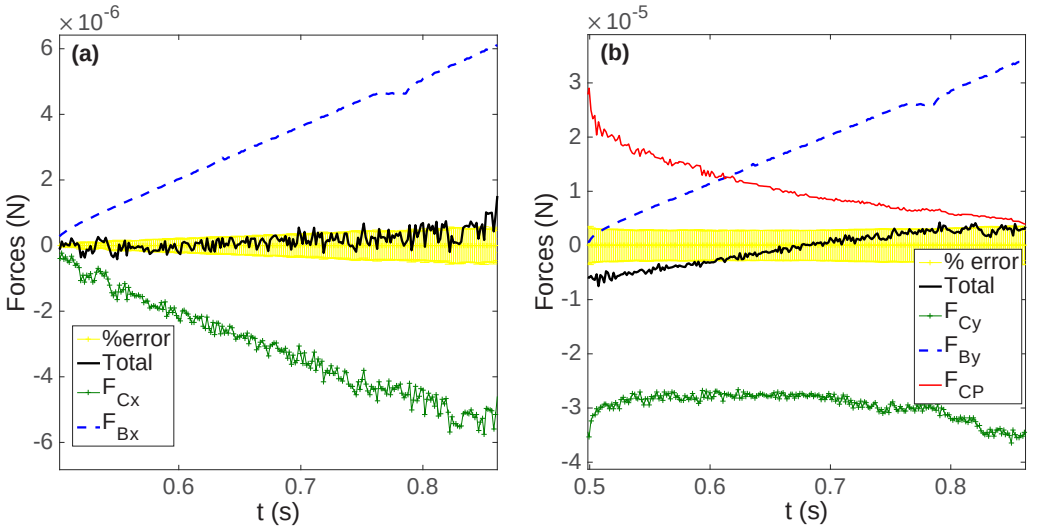

FIG. 9. Force balance in both directions for a tilted surface of 9.5° on treated glass (a) parallel to the wall and (b) perpendicular to the wall.

calculation of volume considers only two forces: the buoyancy force and the capillary force for a contact angle at detachment equal to 90°. However, in our experiment, the contact angle at detachment is close to $\alpha_{\text{det}} = 67°$, 77°, and 40° for Teflon, treated glass, and glass substrates, respectively (the contact angle at detachment was taken just before the neck formation). The correction of Tate's volume by the contact angle $[V_{\text{Tate}} \sin(\alpha)]$ at detachment reduces the error (6%, 7%, or 3%).

B. Small slope of the surface

In some cases (inclined surface or in shear flow, etc.), we must differentiate between the advancing angle α and receding angle β of the bubble. Klausner *et al.* [18] proposed an expression of the capillary force in both directions for a circular bubble foot and a linear evolution of the contact angle between the advancing angle and receding angle:

$$\mathbf{F_{Cx}} = -2r_f\gamma_l \frac{\pi(\alpha-\beta)}{\pi^2-(\alpha-\beta)^2}[\sin(\beta)+\sin(\alpha)]\mathbf{e_x}, \tag{8}$$

$$\mathbf{F_{Cy}} = -2r_f\gamma_l \frac{\pi}{\alpha-\beta}[\cos(\beta)-\cos(\alpha)]\mathbf{e_y}. \tag{9}$$

The results of Klausner *et al.* [18] on numerical integration of the capillary force show that $\mathbf{F_{Cx}}$ given by Eq. (8) must be corrected by a factor of 1.25, while $\mathbf{F_{Cy}}$ does not need correction. For an inclined test bench, we need to evaluate the forces acting on a bubble in both directions (parallel and normal to the plate). In the direction parallel to the plate, the buoyancy acts for bubble detachment against the capillary force. In the direction perpendicular to the plate, the same forces act on the bubble for a tilted bench as for an horizontal bench. The advancing and receding angles of the bubble are different. Equations (8) and (9) for the capillary force are used in the force balance for low inclination (less than 15°). The force balance is verified in both directions for an inclination of 9.5° for the three substrates. Results are plotted for treated glass in Fig. 9. For higher inclinations of the plate (28.4°), the modeling of the capillary force does not allow one to satisfy the force balance as pointed out in Fig. 10.

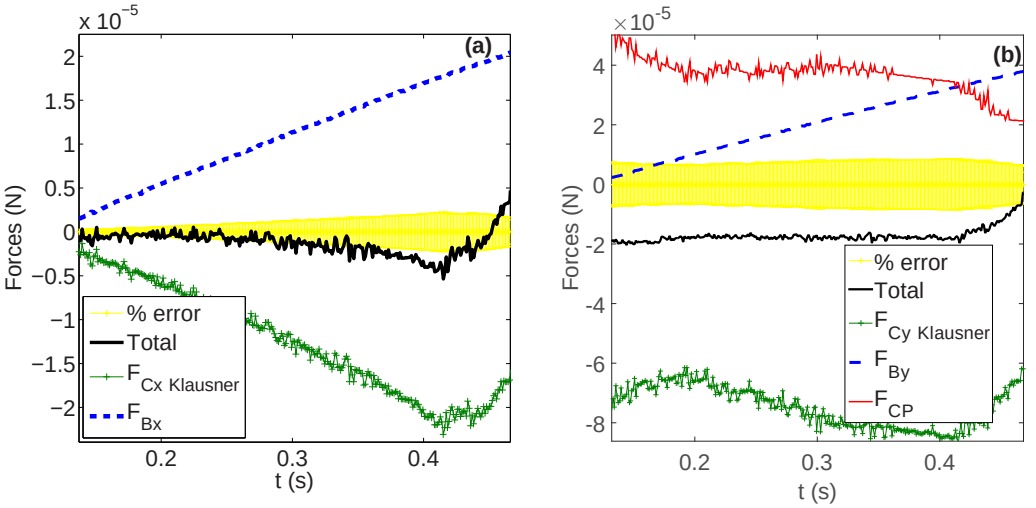

FIG. 10. Force balance in both directions for a treated glass tilted surface of 28.4° on (a) the x component and (b) the y component using Eqs. (8) and (9) for the capillary force.

C. Highly inclined surface

It is observed that when air bubbles grow on an inclined surface, the bubble foot elongates only in the x direction [Fig. 6(b)]. This elongation modifies the capillary force and the contact pressure force and thus the force balance commonly used. This elongation appears to be similar to the studies of Furmidge [19] and Dussan V. *et al.* [20], who studied the different shapes of the foot for a drop or a bubble stuck on a tilted surface. When the inclination of the surface increases, the bubble foot is no longer circular. An elongation is observed in the tangential direction of the plate (cf. Fig. 11).

The capillary force is then changed. Its modeling will depend on the bubble foot shape and the value of the contact angle all along the contact line.

The evolution of the bubble foot elongated radius r_f scaled by the bubble foot radius r_0 at 0° of inclination is plotted versus the surface inclination θ for the three substrates (Fig. 12). In the preceding section we noticed when the slope of the surface is low ($\theta < \theta_{cr} = 15°$) the elongation of the bubble foot is not important enough to modify the capillary force. The bubble foot remains circular and with a radius very close to r_0. When $\theta > \theta_{cr} = 15°$, the bubble elongates only in the direction of the inclination (filmed by camera 1). The elongation ΔL is equal to the difference between the bubble foot radii on the two views. An expression of the bubble foot radius is found versus the bubble foot at $\theta = 0°$ (which is the same whatever the plate inclination on camera 2),

$$r_f = r_0 + \Delta L = r_0[1 + A\mathcal{H}(\theta - \theta_{cr})(\sin\theta - \sin\theta_{cr})], \tag{10}$$

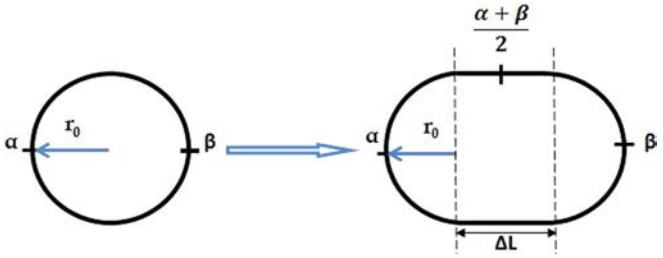

FIG. 11. Shape and settings of the bubble shape.

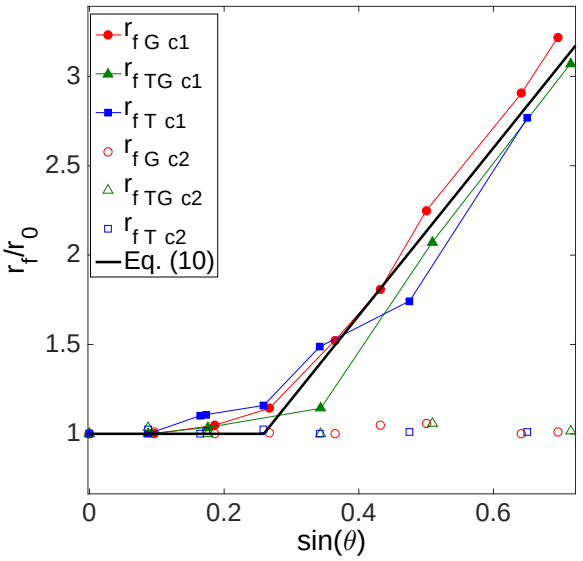

FIG. 12. Evolution of the bubble foot radius r_f scaled by the radius r_0 at 0° of inclination versus the inclination surface θ.

where $A = 4.69$, ΔL is the bubble elongation, and $\mathcal{H}$ is the following Heaviside function, equal to 0 if $\theta < \theta_{cr}$ and equal to 1 if $\theta > \theta_{cr}$.

This elongation is linked to the inclination of the surface. The bubble foot is assumed to follow the contour given in Fig. 11. An additional hypothesis on the contact angle evolution along this contour is required for the modeling of the capillary force. The contact angle is assumed to be constant and equal to $\frac{\alpha+\beta}{2}$ on the straight line segment ΔL (see Fig. 11) and we suppose a linear evolution of the contact angle between the advancing angle α and $\frac{\alpha+\beta}{2}$ and between $\frac{\alpha+\beta}{2}$ and the receding angle β. According to these assumptions, the component of the capillary force perpendicular to the wall is written

$$F_{Cy} = -2r_0\gamma_l \frac{\pi}{\alpha-\beta}[\cos(\beta) - \cos(\alpha)] - 2\Delta L\gamma_l \sin\left(\frac{\alpha+\beta}{2}\right). \tag{11}$$

The component of the capillary force F_{Cx} remains unchanged. Finally, the force balance in the direction parallel to the wall is

$$(\rho_l - \rho_g)V_b g \sin(\theta) - 1.25 \times 2r_0\gamma_l \frac{\pi(\alpha-\beta)}{\pi^2 - (\alpha-\beta)^2}[\sin(\beta) + \sin(\alpha)] = 0. \tag{12}$$

In the perpendicular direction, the force balance becomes

$$(\rho_l - \rho_g)V_b g \cos(\theta) + \frac{2S_f\gamma_l}{R_S} + S_f\rho_l g h - 2r_0\gamma_l \frac{\pi}{\alpha-\beta}[\cos(\beta) - \cos(\alpha)]$$
$$- 2\gamma_l \Delta L \sin\left(\frac{\alpha+\beta}{2}\right) = 0, \tag{13}$$

where $S_f = \pi r_0^2 + 2r_0\Delta L$ is the surface of the bubble foot used in the calculation of the contact pressure force. The force balance for two inclinations on a Teflon plate is plotted in Fig. 13. These different forces show the importance of the boundary conditions at the triple contact line. The force balance is well satisfied in both directions for all the substrates and all the surface inclinations.

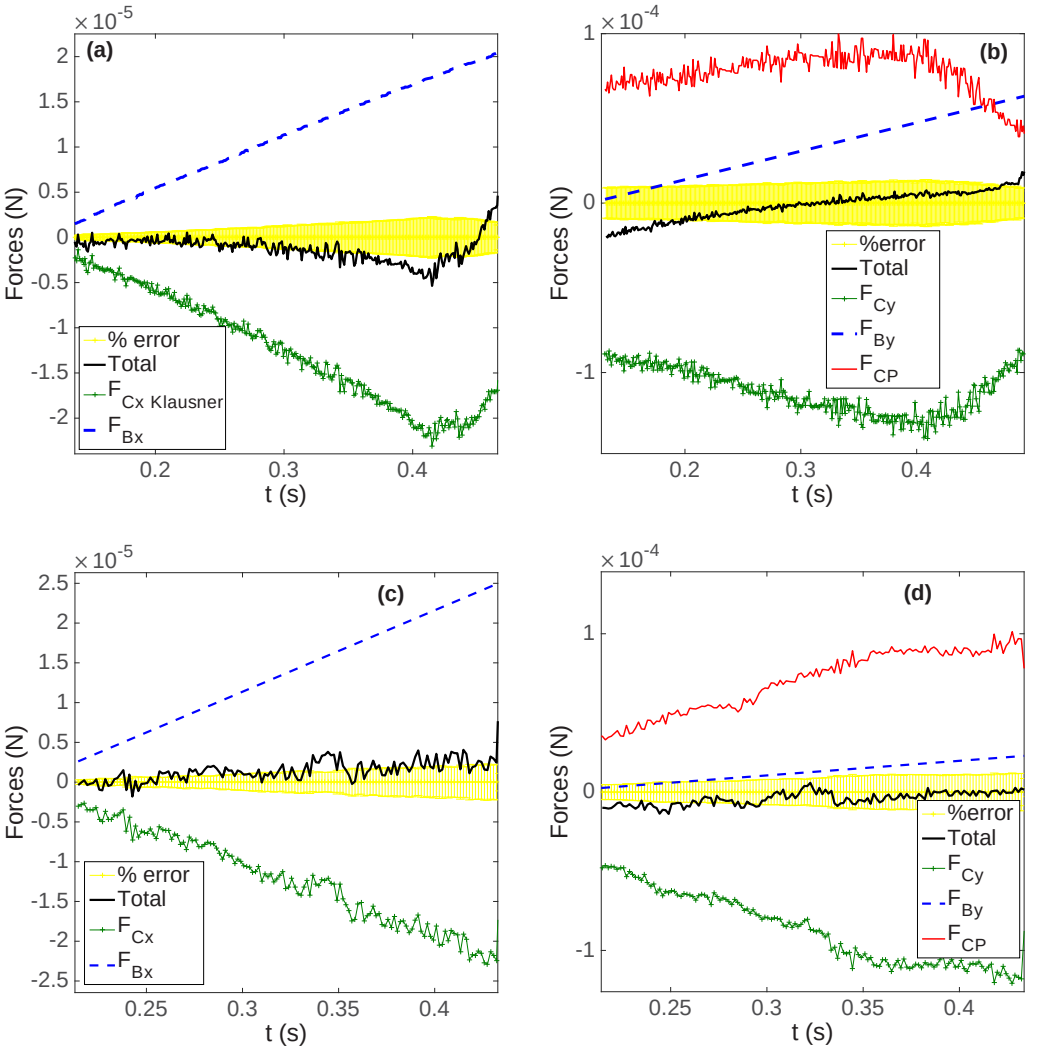

FIG. 13. Force balance on a Teflon plate with elongated bubble foot on an inclined surface of 28.4° (a) parallel to the wall and (b) perpendicular to the wall [Eq. (11)] and on an inclined surface of 50.9° (c) parallel to the wall and (d) perpendicular to the wall [Eq. (11)].

D. Detachment model

In the quasistatic and dynamic regimes, bubble detachment is most of the time predicted from a force balance applied to a bubble assumed to be spherical. Zeng *et al.* [21,22] developed a model (for pool and flow boiling) which simultaneously calculates the bubble diameter and the inclination angle of the bubble at detachment. Duhar and Colin [17] proposed a predictive model of the bubble radius at detachment in a Couette flow for small bubble Reynolds numbers. It is based on the resolution of a system of two equations (momentum balance equations in the directions parallel and perpendicular to the wall). The detachment criterion was based on a given value of the advancing contact angle α and the system of two equations was numerically solved to calculate the two unknowns β and the bubble radius at detachment R_{det}. This model predicts the bubble radius at detachment in a viscous liquid at low air injection rates (less than 40 $\mathrm{mm^3\,s^{-1}}$) and shear rates below 10 $\mathrm{s^{-1}}$. This approach

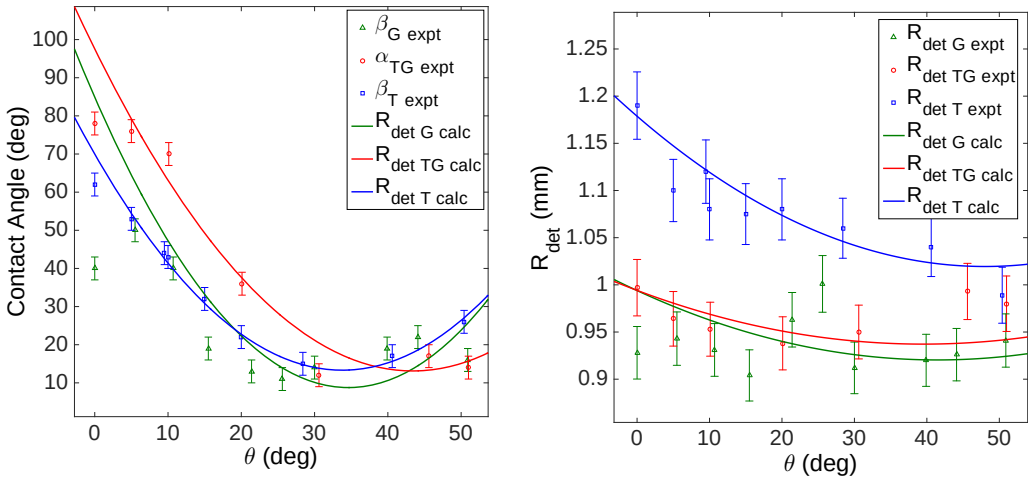

FIG. 14. Evolution of the receding angle and radius at lift-off.

will be applied to predict the bubble detachment diameter on a tilt surface. A criterion for the bubble lift-off based on a critical value of the advancing contact angle is being sought.

We plotted the contact angle values at the bubble detachment versus the inclination angle of the bench for the three substrates (Teflon, treated glass, and glass) in Fig. 6(a). We have the same evolution of the contact angle for all the substrates. The advancing angle α at detachment increases and reaches a quasiconstant value (76° for Teflon, 80° for treated glass, and 70° for glass) for a tilted surface with an angle superior to 10°. The receding angle β decreases [see Fig. 6(a)]. The wettability of the substrates does not have a significant influence on the contact angle at detachment but it affects the value of r_0. At detachment r_0 is about equal to r_c on the glass substrates and to $1.3r_c$ for the Teflon plate. If r_0 and α_{det} are known, Eqs. (12) and (13) are written as follows:

$$(\rho_l-\rho_g)V_b g\sin(\theta)-1.25\times 2r_0\gamma_l\frac{\pi(\alpha_{\text{det}}-\beta)}{\pi^2-(\alpha_{\text{det}}-\beta)^2}[\sin(\beta)+\sin(\alpha_{\text{det}})]=0, \tag{14}$$

$$(\rho_l-\rho_g)V_b g\cos(\theta)+\frac{2S_f\gamma_l}{R_{\text{eq}}}+S_f\rho_l gh-2r_0\gamma_l\frac{\pi}{\alpha_{\text{det}}-\beta}[\cos(\beta)-\cos(\alpha_{\text{det}})]$$
$$-2\gamma_l r_0\{A\mathcal{H}(\theta-\theta_{cr})[\sin(\theta)-\sin(\theta_{cr})]\}\sin\left(\frac{\alpha_{\text{det}}+\beta}{2}\right)=0 \tag{15}$$

At detachment, the bubble is assumed to be spherical ($V_b=\frac{4}{3}\pi R_{\text{det}}^3$, $h=2r_{\text{det}}$, $r_s=r_{\text{det}}$, and $S_f=\pi r_0^2+2r_0\Delta L$). We obtain a system of two equations with the two unknowns: the receding contact angle β and detachment radius R_{det} for a set of parameters (α_{det}, θ, and r_0). We compare the experimental values of bubble radius and receding angle at lift-off and the calculated values from the satisfied force balance. For an inclination angle of the test bench superior to 5°, the model provides a reasonable prediction of the data. Indeed, the calculated values of the two unknowns are in good agreement with the experiments (see Fig. 14). For an inclination of 5°, the advancing angle on the Teflon surface is 65° instead of 80°, the value assumed for the prediction. It is normal that the calculated values do not match the experimental values for this inclination. The same comments can be made for the glass substrates. For this model, the knowledge of r_0 is very important and it is directly linked to the substrate wettability.

V. CONCLUSION

The injection of air bubbles on a tilted plate in a quiescent liquid was studied. Image of bubbles were taken with two perpendicular high-speed cameras. The interface shape of the bubble and geometrical characteristic parameters were determined with image processing software, based on MATLAB. From these parameters, the different forces acting on bubbles in a static regime were quantified. In a quiescent liquid, for an inclination of the surface greater than 20°, an elongation of the bubble foot was noted. The modeling of the capillary force and the contact pressure force was improved and the force balance was satisfied. We proposed the prediction of the bubble radius at detachment with a model based on a force balance and limit values reached by the contact angles. The bubble radius and the receding angle at detachment were well predicted in a quiescent liquid by using Eqs. (12) and (13) for an inclination angle θ between 10° and 50°. The lift-off criterion is based on the contact angles ($\alpha = 70°$, 76°, or 80° for glass, treated glass, and Teflon substrates). Further experiments should be performed to determine the hydrodynamic forces acting on an isolated bubble in a shear flow.

ACKNOWLEDGMENTS

The authors would like to acknowledge the National French Space Agency under convention GDR MFA/CNES 150515/00 and the European Space Agency (ESA) under MAP Project CBC No. 4200020289 for cofunding this study. Grégory Ehses and Sébastien Cazin are thanked for the building of the setup and implementation of the optical bench with the cameras.

[1] R. L. Judd and K. S. Hwang, A comprehensive model for nucleate pool boiling heat transfer including microlayer evaporation, J. Heat Transfer **98**, 623 (1976).
[2] N. Basu, G. R. Warrier, and V. K. Dhir, Wall heat flux partitioning during subcooled flow boiling: Part 1-model development, Trans. ASME J. Heat Transfer **127**, 131 (2005).
[3] H. N. Oguz and A. Prosperetti, Dynamics of bubble growth and detachment from a needle, J. Fluid Mech. **257**, 111 (1993).
[4] E. S. Gaddis and A. Vogelpohl, Bubble formation in quiescent liquids under constant flow conditions, Chem. Eng. Sci. **41**, 97 (1986).
[5] D. Gerlach, G. Biswas, F. Durst, and V. Kolobaric, Quasi-static bubble formation on submerged orifices, Int. J. Heat Mass Transfer **48**, 425 (2005).
[6] S. Di Bari and A. J. Robinson, Experimental study of gas injected bubble growth from submerged orifices, Exp. Therm. Fluid Sci. **44**, 124 (2013).
[7] S. Siedel, S. Cioulachtjian, and J. Bonjour, Experimental analysis of bubble growth, departure and interactions during pool boiling on artificial nucleation sites, Exp. Therm. Fluid Sci. **32**, 1504 (2008).
[8] N. Schweizer and P. Stephan, Experimental study of bubble behavior and local heat flux in pool boiling under variable gravitational conditions, Multiphase Sci. Technol. **21**, 329 (2009).
[9] G. Son, V. K. Dhir, and N. Ramanujapu, Dynamics and heat transfer associated with a single bubble during nucleate boiling on a horizontal surface, J. Heat Transfer **121**, 623 (1999).
[10] C. Kunkelmann and P. Stephan, Numerical simulation of the transient heat transfer during nucleate boiling of refrigerant HFE-7100, Int. J. Refrig. **33**, 1221 (2010).
[11] G. Huber, S. Tanguy, M. Sagan, and C. Colin, Direct numerical simulation of nucleate pool boiling at large microscopic contact angle and moderate Jakob number, Int. J. Heat Mass Transfer **113**, 662 (2017).
[12] A. K. Chesters, Modes of bubble growth in the slow-formation regime of nucleate pool boiling, Int. J. Multiphase Flow **4**, 279 (1978).
[13] T. Tate, On the magnitude of a drop of liquid formed under different circumstances, Philos. Mag. **27**, 176 (1864).

[14] G. E. Thorncroft, J. F. Klausner, and R. Mei, Bubble forces and detachment models, Multiphase Sci. Technol. **13**, 35 (2001).
[15] G. H. Yeoh and J. Y. Tu, A unified model considering force balances for departing vapour bubbles and population balance in subcooled boiling flow, Nucl. Eng. Des. **235**, 1251 (2005).
[16] A. F. Stalder, T. Melchior, M. Müller, D. Sage, T. Blu, and M. Unser, Low-bond axisymmetric drop shape analysis for surface tension and contact angle measurements of sessile drops, Colloids Surf. A **364**, 72 (2010).
[17] G. Duhar and C. Colin, Dynamics of bubble growth and detachment in a viscous shear flow, Phys. Fluids **18**, 077101 (2006).
[18] J. F. Klausner, R. Mei, M. D. Bernhard, and L. Z. Zeng, Vapor bubble detachment in forced convection boiling, Int. J. Heat Mass Transfer **36**, 651 (1993).
[19] C. G. L. Furmidge, Studies at phase interfaces. I. The sliding of liquid drops on solid surfaces and a theory for spray retention, J. Colloid Sci. **17**, 309 (1962).
[20] E. B. Dussan, V. Chow, and R. Tao-Ping, On the ability of drops or bubbles to stick to non-horizontal surfaces of solids, J. Fluid Mech. **137**, 1 (1983).
[21] L. Z. Zeng, J. F. Klausner, and R. Mei, A unified model for the prediction of bubble detachment diameters in boiling systems–1. Pool boiling, Int. J. Heat Mass Transfer **36**, 2261 (1993).
[22] L. Z. Zeng, J. F. Klausner, D. M. Bernhard, and R. Mei, A unified model for the prediction of bubble detachment diameters in boiling systems–2. Flow boiling, Int. J. Heat Mass Transfer **36**, 2271 (1993).